Polyploid tubular cells initiate a TGF-β1 controlled loop that sustains polyploidization and fibrosis after acute kidney injury

Letizia De Chiara[1]*, Roberto Semeraro[2], Benedetta Mazzinghi[3], Samuela Landini[4], Alice Molli[3], Giulia Antonelli[1], Maria Lucia Angelotti[1], Maria Elena Melica[1], Laura Maggi[2], Carolina Conte[1], Anna Peired[1], Luigi Cirillo[3], Valentina Raglianti[1], Alberto Magi[5], Francesco Annunziato[2,6], Paola Romagnani[1,3] and Elena Lazzeri[1]*.

Affiliations

[1]Department of Experimental and Clinical Biomedical Sciences "Mario Serio", University of Florence; Florence 50139, Italy.

[2]Department of Experimental and Clinical Medicine, University of Florence; Florence 50139, Italy.

[3]Nephrology and Dialysis Unit, Meyer Children's University Hospital, IRCCS; Florence 50139, Italy.

[4]Medical Genetics Unit, Meyer Children's University Hospital, IRCCS; Florence 50139, Italy.

[5]Department of Information Engineering, University of Florence; Florence 50139, Italy

[6]Flow Cytometry Diagnostic Center and Immunotherapy (CDCI), Careggi University Hospital; Florence 50134, Italy.

***Corresponding Authors:** letizia.dechiara@unifi.it and elena.lazzeri@unifi.it

Running title: Polyploid tubular cells promote fibrosis *via* TGF-β1.

Keywords: Polyploidy, tubular epithelial cells, TGF-β1, CKD, fibrosis

Supplemental Material available at

URL number: https://figshare.com/s/4eda5e9e97ba3bd2c469

DOI number: https://doi.org/10.6084/m9.figshare.22200187.

Abstract

Polyploidization of tubular cells (TC) is triggered by Acute Kidney Injury (AKI) to allow survival in the early phase after AKI, but in the long run promotes fibrosis and AKI-chronic kidney disease (CKD) transition. The molecular mechanism governing the link between polyploid TC and kidney fibrosis remains to be clarified. In this study, we demonstrate that immediately after AKI, expression of cell cycle markers mostly identifies a population of DNA damaged polyploid TC. Employing transgenic mouse models and single cell RNA-sequencing we show that, unlike diploid TC, polyploid TC accumulate DNA damage and survive, eventually resting in G1 phase of the cell cycle. *In vivo* and *in vitro* single cell RNA-sequencing along with sorting of polyploid TC show that these cells acquire a pro-fibrotic phenotype culminating in TGF-β1 expression and that TGF-β1 directly promotes polyploidization. This demonstrates that TC polyploidization is a self-sustained mechanism. Interactome analysis by single cell RNA-sequencing revealed that TGF-β1 signaling fosters a reciprocal activation loop among polyploid TC, macrophages and fibroblasts to sustain kidney fibrosis and promote CKD progression. Collectively, this study contributes to the ongoing revision of the paradigm of kidney tubule response to AKI, supporting the existence of a tubulointerstitial crosstalk mediated by TGF-β1 signaling produced by polyploid TC following DNA damage.

New and Noteworthy

Polyploidization in tubular epithelial cells has been neglected until recently. Here, we showed that polyploidization is a self-sustained mechanism that plays an important role during chronic kidney disease development, proving the existence of a crosstalk between infiltrating cells and polyploid tubular cells. This study contributes to the ongoing revision of kidney adaptation to injury, posing polyploid tubular cells at the center of the process.

Introduction

Acute Kidney Injury (AKI) is characterized by a sudden kidney failure accompanied by a transient and persistent decrease of kidney functionality (1). It is regarded as an important risk factor for chronic kidney disease (CKD) development. Renal fibrosis, especially tubulointerstitial fibrosis, is the final manifestation of CKD (2, 3) and is characterized by an excessive synthesis and deposition of extracellular matrix (ECM) associated with inflammatory infiltration, tubular epithelial cell (TC) damage, fibroblast activation and microvasculature rarefaction (3). Although no targeted therapy yet exists to slow the progression of tubulointerstitial fibrosis (3), recent findings contributed to clarify the cellular and molecular mechanisms underlying its development and progression, posing TC at the center of this process (4-6). Accordingly, we have demonstrated that fibrosis and senescence are trade-offs of TC polyploidy occurring immediately after AKI to support fast kidney function recovery, but promoting consequent CKD (4). However, the mechanisms turning TC polyploidy to senescence and fibrosis still need to be elucidated. Among the many pathways controlling fibrosis deposition, a prominent role is played by the transforming growth factor-β1 (TGF-β1) (7). TGF-β1 is a pleiotropic cytokine which is involved in regulating a broad range of cellular processes (7, 8). In the liver, TGF-β1 is a major inducer of hepatocyte polyploidization (9) and polyploid megakaryocytes are the primary source of TGF-β1 in patients with primary myelofibrosis (10), suggesting the existence of a regulatory loop between fibrosis and polyploidization (10). Additionally, DNA damage and genome instability were shown to trigger TGF-β1 production initiating a vicious circle that leads to fibroblast activation and fibrosis development in the intestine (11).

Here, we aimed to investigate the role of polyploid TC in promoting tubulointerstitial fibrosis and CKD. By employing single cell RNA-sequencing (scRNA-seq) analysis *in vitro* and *in vivo*, as well as transgenic mice and *in vitro* culture, we observed that accumulation of DNA damage in polyploid TC

progressively increases after injury, culminating in the acquisition of a pro-fibrotic profile and of TGF-β1 expression that maintains TC polyploidization *via* YAP1. Moreover, an interactome analysis along with *in vitro* experiments, revealed the existence of a progressive crosstalk between polyploid TC, macrophages and fibroblasts, mediated by TGF-β1 signaling. Collectively, these findings contribute to the ongoing revision of the paradigm of kidney tubule response to AKI, supporting the existence of a tubulointerstitial crosstalk mediated by TGF-β1 signaling produced by polyploid TC following DNA damage.

Materials and Methods.

Mice

To visualize the cell cycle progression of Pax8+ TC, the Pax8.rtTA;TetO.Cre;R26.FUCCI2aR (Pax8/FUCCI2aR) mouse model was employed. This model was obtained by crossing Pax8.rtTA;TetO.Cre mice (4, 12) with mice harboring the Fluorescent Ubiquitin-based Cell cycle Indicator (FUCCI2aR) Cre-dependent reporter (European Mouse Mutant Archive (EMMA), INFRAFRONTIER-I3, Neuherberg-München, Germany), which consists of a bicistronic Cre-activable reporter of two fluorescent proteins whose expression alternates based on cell cycle phase: mCherry-hCdt1 (30/120) (red), expressed by nuclei of cells in G1 phase, and mVenus-hGem (1/110) (green), expressed by nuclei of cells in S/G2/M. Cells can also appear as yellow at the G1/S boundary (13). Mice were developed on a full C57Bl/6 background (4, 12). Reporter expression was induced in male mice at 5 weeks of age with doxycycline treatment for 10 days followed by one week of washout as previously described (4, 12). After that, mice underwent a unilateral ischemia reperfusion injury (uni-IRI) of 30 min, and were then sacrificed at day 2 and 30 after uni-IRI. Sham operated mice were used as controls. Animal experiments were approved by the Institutional Review Board and by the Italian Ministry of Health and performed in accordance with institutional, regional, and state guidelines and in adherence to the National Institutes of Health Guide for the Care and Use of Laboratory Animals. Mice were housed in a specific pathogen-free facility with free access to chow and water and a 12-hour day/night cycle. The references to the ethics approvals are the following: 689/2019-PR and 864/2021-PR.

Genotyping

Genotyping was performed as previously shown (4, 12). In brief, tail biopsies were incubated overnight at 55 °C in lysis reagent, centrifuged and DNA extracted using isopropanol (Merck). Primers and PCR

parameters were obtained from Jackson Laboratory online resources of the relative strain purchased or previously reported experimental procedure (4).

Unilateral ischemia reperfusion injury

Renal ischemia was performed on male mice as previously described (4, 12, 14). Briefly, mice were anesthetized and the left kidney was then externalized and the renal artery was clamped for 30 min. After clamp removal, the muscle layer was sutured, followed by the closure of the skin wound with metal clips. Sham-operated mice underwent the same surgical procedure without left renal artery clamping.

Blood urea nitrogen quantification

Kidney function was assessed at different time points by collecting a small amount of blood from mice with a metal lancet from the submandibular plexus in order to measure BUN levels. Blood parameters were measured in EDTA anticoagulated plasma samples using Reflotron (Roche Diagnostics), according to the manufacturer's protocols.

FACS analysis on mouse kidney

Cell cycle analysis was performed on total FUCCI2aR cells (mCherry+ and mVenus+ cells). Kidneys were processed to obtain a single cell suspension as previously reported (4, 12). Briefly, kidneys were minced and the digested kidneys were centrifuged, digested and stained as previously shown (4, 12). Cells were then incubated with DAPI (4′,6-diamidino-2-phenylindole, 1:2000, Thermo Fisher Scientific), to perform the DNA content analysis. The assessment of polyploid TC was performed using a MacsQuant instrument (Miltenyi Biotec). Anti-DsRed pAb (Clontec, 632496) was employed to mark mCherry+ TC followed by incubation with Alexa Fluor 647 secondary antibody; mVenus+ TC were identified following incubation with anti-GFP-488 pAb (Thermo Fisher Scientific, A21311). Polyploid TC were defined as mCherry+ or mCherry+mVenus+ cells with a DNA content ≥4C and mVenus+ with a DNA content ≥8C. To detect mVenus+ TC with DNA damage, γH2AX (Thermo Fisher

Scientific, 14-9865-82) was incubated for 1h followed by anti-mouse IgG1 Alexa Fluor 647 secondary antibody. To detect mCherry+ TC with DNA damage, γH2AX was incubated for 1h followed by anti-mouse IgG1 Alexa Fluor 488 secondary antibody. Cells were then incubated with DAPI to perform the DNA content analysis. The percentage of polyploid and diploid TC with DNA damage was calculated on the total % of mVenus+ or mCherry+ cells. Diploid *vs* polyploid fraction was determined based on DNA content. Specifically, mCherry+ TC with 2C DNA content or mVenus+ TC with up to 4C DNA content were considered diploid cells. mCherry+ TC with ≥4C DNA content or mVenus+ TC with ≥8C DNA content were considered polyploid cells. Alexa Fluor 647 secondary antibody was excited by a 633 nm laser line, GFP was excited by a 488 nm laser line, DAPI was excited by a laser at 405 nm. Gating strategy to exclude cell doublets was performed as previously published (4). All isotype controls are shown in Supplemental Fig. S1, S3 and S5 (https://figshare.com/s/4eda5e9e97ba3bd2c469). Data were analysed by FlowLogic software (FlowLogic 7.2.1, Inivai Technology).

hPTC culture, virus transduction, Fluorescence-activated cell sorting, TGF-β1, Verteporfin and Fresolimumab treatments

Human proximal tubular cells (hPTC) (ATCC-PCS-400-010) were maintained in REGM (Lonza, CC-3190). hPTC were seeded at a density 10^5 cells/6-well. The following day cells were transduced with a pRetroX-G1-Red (Clontech, 631436) to allow the identification of cells in G1 phase. A MOI of 10 was used (Retro-X™ qRT-PCR Titration Kit, 631453) according to manufacturer's instruction. In this plasmid the cell cycle indicator hCdt1 (30-120) is tagged with the red fluorescent protein mCherry. After transduction, cells are referred to as hPTC-mCherry. These cells were trypsinized (Euroclone) at passage 2 after transduction, fixed and stained for FACS as previously described (4). To detect mCherry+ hPTC, cells were incubated with anti-DsRed (1:25, Clontech, 632496) or isotype control and then incubated with Alexa Fluor 647 goat anti-rabbit (1:100, Thermo Fisher Scientific, A-21245).

hPTC were then incubated with DAPI (1:2000, Thermo Fisher Scientific) to perform the DNA content analysis and analysed on MacsQuant instrument (Miltenyi Biotec). In the verteporfin experiment, Alexa Fluor 488 goat anti-rabbit (1:100, Thermo Fisher Scientific, A21311) was employed. Alexa Fluor 488 secondary antibody was excited by a 488 nm laser line, Alexa Fluor 647 secondary antibody was excited by a 635 nm laser line, DAPI was excited by a 405 nm laser line. Cell cycle analysis and gating strategy to exclude cell doublets was performed on total hPTC as previously published (4). Polyploid hPTC were defined as mCherry+ cells with a DNA content ≥4C. In the sorting experiment, the same protocol was applied but all the antibodies were diluted in 0,5% saponin (Merck) with the addition of 1:100 RNAase inhibitor (Applied Biosystems, N8080119). The solutions were prepared in RNAase-free PBS and the procedure was carried out on ice. Following DAPI incubation, hPTC were sorted on the FACSAria III BD (Bioscience). Alexa Fluor 647 secondary antibody was excited by a 633 nm laser line, DAPI was excited by a 405 nm laser line. Data were analysed by FacsDiva software (Beckman Coulter). In additional experiments, cells were seeded and the day after treated with TGF-β1 (Peprotech) at concentration of 10ng/ml or vehicle (10nM citric acid). Fresolimumab (HY-P99020, DBA dissolved in DMSO) was incubated at the concentration of 10µg/ml (15) for 1h prior to TGF-β1 stimulation. DMSO (Merck) was used as vehicle control. Effective block of TGF-β1 pathway activation was tested by incubating hPTC with Fresolimumab or vehicle control for 48h. Cells were then harvested followed by RNA extraction and RealTime analysis of relevant targets was performed. For verteporfin treatment (Biotechne, 5305), cells were stimulated with a verteporfin concentration of 0.6 µM 1h prior TGF-β1 treatment. Cells were then harvested after 48h. DMSO (Merck) was used as vehicle control. After 48 h, hPTC-mCherry were trypsinized (Euroclone) and analysed at FACS. All isotypes controls are shown in Supplemental Fig. S5 (https://figshare.com/s/4eda5e9e97ba3bd2c469).

Human Monocyte purification

Monocytes CD14+ were positively selected by magnetic cell sorting MACS (Miltenyi Biotec) from PBMNC (Peripheral blood Mononuclear Cells) derived from buffy coats of healthy donors, accordingly to manufacturing instructions. Purity of CD14+ cells was checked by flow cytometry staining (BD LSR II) and it was > 95%. CD14+ cells were resuspended in RPMI (BioConcept) plus 5% FCS for co-culture experiments.

In vitro macrophage differentiation

Monocytes CD14+ previously purified form PBMNC of healthy subjects were cultured *in vitro* to obtained macrophages. $3x10^6$ cells/well were cultured in RPMI plus 5% FCS in a 6-well plate in the final volume of 6 ml/well in presence of GM-CSF 10ng/ml (7954-GM, R&D Systems) and placed in incubator at 37°C, 5% CO2. At day 5, culture supernatant was removed and adherent cells were recovered with cold PBS. Macrophage phenotype was checked by flow cytometry staining (BD LSR II) for scatter parameters and for the expression of CD14, CD16, CD80, CD84, CD64 and HLA-DR (Supplemental Fig. S8). Macrophages were resuspended in RPMI plus 5% FCS for co-culture experiments.

Co-culture experiments

hPTC were seeded at a density of $25x10^3$ cells/24-well. The day after hPTC were stimulated with TGF-β1 for 24h, or treated with hydrogen peroxide (0.5μM, Merck) for 1h to mimic hypoxia. After stimulation, the medium was removed, washed once with PBS and fresh medium was added. Human primary fibroblasts were seeded at a density of 10^4 cells on transwell permeable supports with pore sizes of 8 μm (Corning). After 24h of incubation, cells were harvested, RNA was extracted and analyzed by Real-Time PCR. For the monocytes and macrophages co-cultures, hPTC were seeded at a density of $1x10^5$ cells/6-well. After stimulation as described above, $1x10^6$ monocytes or macrophages were seeded on transwell permeable supports with pore sizes of 3μm (Corning).

Quantitative Real-Time PCR

Total RNA from sorted cells and total mCherry-hPTC was extracted using RNeasy Microkit (Qiagen) and retrotranscribed using TaqMan Reverse Transcription Reagents (Thermo Fisher Scientific). TaqMan RT-PCR for 18S, TGF-β1, SMAD2, SMAD3, CTGF, VIMENTIN, MAF, HIF1α, IL6, CCL2 and p21 was performed using customized TaqMan assays (Thermo Fisher Scientific) on a 7900HT Fast Real-Time (Applied Biosystem). ΔΔCT was used to calculate relative quantification.

Single-cell data analysis

Two previously published datasets (GSE212273, GSE212275) containing single-cell data generated on mouse kidneys at 2 and 30 days after uni-IRI, and hPTC respectively, were re-analyzed to investigate the mechanisms linking polyploid TC to kidney fibrosis (4).

We started from the mice dataset (GSE212273) that integrates samples from three experimental points t0, t2 and t30. In order to study events happening between t2 and t30, by means of Scanpy framework, we loaded the dataset, removed the t0 samples and recalculated the neighborhood graph on the latent space in order to cluster and annotate the resulting data.

Next, we annotated the new dataset, adding information obtained from the proximal TC analysis described in our previous work (4, 12). In particular, we looked for cells belonging to proximal clusters 8 and 9, as defined in the previous paper, and we labeled cells in the new dataset as 8 or 9 based on the origin proximal cluster. As result, we identified polyploid cells in the new dataset, that we used for the interactome analysis.

The human dataset (GSE212275), was loaded in Scanpy. We focused our analysis on polyploid clusters 4, 5, 7, 9 and 10 as previously demonstrated and described elsewhere (4). We further generated and analyzed a new dataset containing hPTC stimulated with TGF-β1 or vehicle treated cells. To start, raw sequencing data were processed using the 10x Genomics Cell Ranger pipeline (version 3.0.1). First, cellranger mkfastq demultiplexed libraries based on sample indices and converted the barcode and read

data to FASTQ files. Second, cellranger count took FASTQ files and performed alignment to the human GRCh38 reference genome, to then proceed with filtering and unique molecular identifier (UMI) counting. Next, we loaded the count matrix in Scanpy to proceed with quality control. After filtering, we obtained 10402 cells with less than 25% of mitochondrial read rate and expressing more than 2000 genes. Cell-specific biases were normalized by dividing the measured counts by the size factor obtained through the scran computeSumFactors method, which implements the deconvolution strategy for scaling normalization (4). Finally, all counts were log-transformed after addition of a pseudocount of 1. Next, we mitigated the batch effect through the matching mutual nearest neighbors (MNN) algorithm to later proceed with feature selection to keep "informative" genes only, used for dimensional reduction through PCA. The first 50 principal components (PCs) were used to construct a neighborhood graph of observations through the pp.neighbors function, which relies on the Uniform Manifold Approximation and Projection (UMAP) algorithm to estimate connectivity of data points. Cell cycle analysis was performed by creating two lists of genes associated to the S and G2/M phases based on cell cycle genes previously defined (16), passed to the tl.score_cell_cycle_genes function to score S and G2/M phases. Next, we clustered data by tl.louvain function at different resolutions (0.5, 1) and 1 proved to be the best, producing ten clusters of hPTC. To annotate the clusters we ran the tl.rank_gene_groups function using the Wilcoxon rank-sum method, to define the marker genes of each cluster. The same was conducted for the treated and untreated cells, to define the marker gene sets of each group and use them for a gene set enrichment anlysis (GSEA), conducted through the prerank function implemented in the gseapy python library (17), that we used to query the MSigDB_Hallmark_2020 database.

Mouse interactome analysis

The mouse datasets prepared before was used to conduct an interactome analysis with CellPhoneDB 4.0.0, through the command: cellphonedb method statistical analysis meta.tsv counts.tsv, where

245 ‘meta.tsv’ correspond to the metadata, reporting the cell types have been exported, and ‘counts.tsv’ to
246 the normalized read counts file. The ouputs produced by CellPhoneDB for the t2 and t30 data, and
247 stored in two “significant means.txt” files, were loaded as pandas dataframes in a python environment
248 (https://pandas.pydata.org) and analyzed separately.
249 The dataframes report the interactions observed between each cell type (rows), at the two experimental
250 points, respectively. The interactions are defined based on the co-expression of a “ligand” molecule in
251 a cell type, defined source, and a “receptor” molecule in another one, defined target. In order to
252 produce a matrix reporting all “as-source” and “as-target” interactions for each cell type, we extended
253 both dataframes adding a source and a target column, which allowed us to obtain pivot tables reporting
254 the number of interactions between “as-source” (rows) and “as-target” (columns) cell types. With these
255 tables we computed the Spearman’s Rank Correlation for rows and columns. Next, we used each data
256 frame to obtain “as-source” and “as-target” interaction profiles for each cell type. To this aim, we
257 merged the “as-source” (or “as-target”) cell types with the interaction ids (CPI-SC03515B178),
258 producing a matrix made by columns consisting in the specific interactions of each cell type (CPI-
259 SC03515B178Proximal Tubule) and rows consisting in the cell types. This matrix allowed us to
260 understand if an interactions observed in a specific cell type was also present in another or not, and
261 consequently define specific cell type interaction profiles. Also in this case we computed the
262 Spearman’s Rank Correlation for rows and columns.
263 Finally, we encoded the interaction sets as multi-partite graphs, defined as a 3-tuple G = (C,M,E),
264 where C are the cell types, M the molecules (ligand/receptors), and E the edges connecting the
265 elements of the graph. To generate such a graph, we iterated over the rows of the dataframe and added
266 each interaction as a path, defined as a sequence of edges connecting a source cell (e.g. Proximal
267 Tubule) to a ligand (e.g. FLT1), a ligand to a receptor (e.g. VEGFB), and a receptor molecule to a
268 target cell (e.g. Endothelial).

CellPhoneDB classify interactions in directed if one of the partners was a ligand and the other was a receptor, and undirected otherwise. In this graph we preserved this classification producing a single path (e.g. Proximal Tubule, FLT1, VEGFB, Endothelial) if directed and two paths, one reversed, if not. For each edge, a 'weight' W was defined to encode the total number of occurrences of the corresponding interactions in the interactome. The two paths of an undirected interaction are counted only once for the purpose of computing W. The networks were assembled using the NetworkX library (18), and analysed with the graph algorithms implemented in the library. To compute the centrality measures we used the the degree_centrality, in_degree_centrality and out_degree_centrality functions. The betweenness centrality was calculated through the betweenness_centrality function, using the inverse of the edge weights as a distance measure; the katz_centrality numpy function was used to compute the katz centrality, with the edge weights as the weight measure, and the attenuation factor α as the reciprocal of the absolute value of the largest eigenvalue of the network adjacency matrix.

Finally, by comparing the day 2 and day 30 interactomes we defined the absent, stable, lost and gained interactions for each cell population. Processing this data as a network, we defined the top changing reactions from day 2 to day 30.

Statistical analysis

Comparison between groups was performed by the Mann-Whitney test or Student's t-test. A p-value < 0.05 was considered statistically significant. Statistical analysis was performed using OriginPro (RRID:SCR_015636) statistical software.

Results

Polyploid TC with DNA damage accumulate after injury *in vivo*. After AKI, a subset of polyploid TC, undergoes continuous endoreplication cycles and become senescent and pro-fibrotic over time (4). These TC can be identified combining the detection of cell cycle phases using the FUCCI2aR technology with the quantification of the DNA content (4, 12) (Supplemental Fig. S1 and S2 https://figshare.com/s/4eda5e9e97ba3bd2c469). To dissect the mechanisms linking cycling polyploid TC to kidney fibrosis, we re-analyzed the datasets generated on mouse kidneys at 2 (acute phase) and 30 days (chronic phase) after unilateral ischemic reperfusion injury (uni-IRI), restricting our analysis to proximal TC (PTC) and in particular to the clusters we have shown to be polyploid (GSE212273) (4) (Fig. 1A). Louvain clustering showed the presence of 10 clusters and cluster 8 and 9 represented polyploid TC (4) (Fig. 1A). Interestingly, the analysis of cell cycle distribution showed that cluster 9 was mostly composed by polyploid PTC at day 30 in the G1 phase of the cell cycle (Fig. 1A, B). Conversely, cluster 8 was mostly composed by polyploid PTC at day 2 (Fig. 1A, B) that appeared to be actively cycling based on cell cycle scoring algorithm (16) (Fig. 1A) and on the expression of traditional cell cycle activation markers (Pcna) and G2/M phase markers (Aurkb) (Fig. 1C, D). Polyploid cluster 8 was further characterized by both polyploidy regulators (E2f1, E2f7, E2f8, Ccne1, Ccne2, Cdk1) and cell cycle inhibitors such as p21 (Cdkn1a) and p19 (Cdkn2d) genes, proving that this cluster was not actively proliferating but rather undergoing polyploidization (Fig. 1E). This result demonstrates that traditional cell cycle markers identify a polyploid TC population at day 2 after AKI. As p21 expression was shown to be induced in DNA damaged cells (6), we analyzed the expression of a panel of DNA damage markers (Fig. 1F-H). Among those, H2afx was also primarily restricted to cluster 8 (Fig. 1F), demonstrating that DNA damaged TC mostly undergo endoreplication mediated-polyploidization after AKI. To confirm this observation, we took advantage of our model of Pax8/FUCCI2aR mice, where polyploid TC can be identified as mCherry+ TC with ≥4C DNA content

313 (polyploid TC in G1 phase) or mVenus+ with ≥8C DNA content (polyploid TC in G2/M phase), as
314 previously described (4) and shown in Supplemental Fig. S2C, D
315 (https://figshare.com/s/4eda5e9e97ba3bd2c469). Importantly, we found that the percentage of TC with
316 DNA damage (TC positive for γH2AX) significantly increased among the polyploid TC in G2/M phase
317 (mVenus+ with ≥8C DNA content) in comparison to proliferating diploid TC (mVenus+ with a DNA
318 content =4C) at day 2 after uni-IRI, but decreased 30 days after uni-IRI (Fig. 1I, J and Supplemental
319 Fig. S3 https://figshare.com/s/4eda5e9e97ba3bd2c469). This indicates that immediately after AKI,
320 DNA damage accumulates in polyploid, but not in truly proliferating TC. Conversely, the percentage of
321 G1 polyploid TC with DNA damage (TC positive for γH2AX) progressively increased 30 days after
322 uni-IRI (mCherry+ TC with ≥4C DNA content) (Fig. 1K, L and Supplemental Fig. S3
323 https://figshare.com/s/4eda5e9e97ba3bd2c469), suggesting that after AKI polyploid TC with DNA
324 damage progressively accumulate and rest in the G1 phase of the cell cycle. By contrast, no significant
325 upregulation of γH2AX was found in diploid TC (mCherry+ with a DNA content =2C) (Fig. 1L).
326 Consistently, polyploid TC with a ≥8C DNA content has significantly increased at day 30 after AKI,
327 suggesting that polyploid TC with DNA damage undergo further endoreplication cycles to promote
328 polyploidization overtime (Supplemental Fig. S2D https://figshare.com/s/4eda5e9e97ba3bd2c469).
329 Taken altogether, these results demonstrate that 1. Expression of G2/M cell cycle markers in the acute
330 phase of injury response characterizes endoreplicating rather than proliferating TC; 2. Polyploid TC but
331 not diploid TC accumulate DNA damage in the acute phase after injury, progressively increase
332 overtime and finally stall in the G1 phase of cell cycle, suggesting that DNA damage stimulates TC to
333 undergo endoreplication cycles becoming polyploid.
334
335 **Polyploid TC are pro-fibrotic and actively produce TGF-β1 *in vitro*.** To dissect the link between
336 polyploid TC with DNA damage and fibrosis development, we analyzed the expression of genes

known to be involved in the development of fibrosis on mouse kidneys at 2 and 30 days after uni-IRI. Importantly, G1 polyploid TC at day 30 after uni-IRI appear to express TGF-β1 and its receptor (TGF-βR2, Fig. 2A, B), indicative of an acquired pro-fibrotic state. Conversely, diploid TC were not characterized by TGF-β1 expression (Supplemental Fig. S4A https://figshare.com/s/4eda5e9e97ba3bd2c469). Likewise, a re-analysis of the dataset (GSE212273) of human proximal tubular cell (hPTC), which we have found to contain a fraction of polyploid hPTC (4), showed similar results (Fig. 2C-F). Unsupervised clustering of primary hPTC showed the presence of eleven clusters, and clusters 4, 5, 7, 10 and 9 were identified as polyploid clusters based on the expression of characteristic genes involved in TC polyploidization (4, 19) (Fig. 2C). In agreement with what we had observed *in vivo*, polyploid clusters were characterized by cell cycle activation markers (Pcna, Aurkb), polyploidy regulators (E2f1, E2f7, E2f8, Ccnb1, Cdk1) (Fig. 2D, E and Supplemental Fig. S4B https://figshare.com/s/4eda5e9e97ba3bd2c469) along with the DNA damage marker, H2afx, confirming that DNA damage accumulates preferentially in polyploid TC (Fig. 2F). This proves that *in vitro* polyploid TC can be successfully employed to mimic the *in vivo* setting. To verify if polyploid TC actively produce TGF-β1, we transduced hPTC with a mCherry-G1 vector to identify cells in the G1 phase (Fig. 2G-J), as previously described (4). Upon transduction, hPTC express the fluorescent protein mCherry (red) in the nuclei of cells in G1 (from now on indicated as mCherry-hPTC), allowing to discriminate G1-polyploid cells (mCherry-hPTC with ≥4C DNA content) from G1-diploid cells (mCherry-hPTC with 2C DNA content) (Fig. 2G-J and Supplemental Fig. S5A-C https://figshare.com/s/4eda5e9e97ba3bd2c469). Importantly, a marked upregulation of mRNA expression of fibrogenic growth factor encoding TGF-β1 was observed in sorted polyploid mCherry-hPTC in comparison to diploid mCherry-hPTC (Fig. 2K). Collectively, these data validate the results observed *in vivo* and demonstrate that G1 resting polyploid TC actively produced TGF-β1.

Polyploidization is a self-sustained mechanism stimulated by TGF-β1. As polyploid TC with DNA damage progressively increase overtime along with an increase in TGF-β1 expression, we investigated whether TGF-β1 directly promotes polyploidization. To this aim, we performed scRNA-seq analysis on hPTC stimulated with TGF-β1 or vehicle. Following TGF-β1 stimulation, hPTC expressed TGF-β1 and its downstream targets as expected (Fig. 3A, B and Supplemental Table S1 https://figshare.com/s/4eda5e9e97ba3bd2c469). Moreover, TGF-β1-treated hPTC were characterized by a differential expression of pro-fibrotic genes (Supplemental Table S1, light yellow genes https://figshare.com/s/4eda5e9e97ba3bd2c469), which we had recently showed to be characteristic of polyploid hPTC and were enriched with hypertrophy genes (Supplemental Table S1, light blue genes https://figshare.com/s/4eda5e9e97ba3bd2c469), indicative of polyploidization. Consistently, a gene set enrichment analysis, confirmed the activation of TGF-β and AKT pathways (Fig. 3C, D), which we have showed to be a key player in TC polyploidization (4). To definitely prove that TGF-β1 stimulates the acquisition of polyploidization, we then treated mCherry-hPTC with TGF-β1 for 48h and observed that the fraction of polyploid TC significantly increased in comparison to vehicle treated hPTC (Fig. 3E-J and Supplemental Fig. S5D-I, https://figshare.com/s/4eda5e9e97ba3bd2c469) proving that TGF-β1 stimulates hPTC polyploidization. Consistently, treatment of mCherry-hPTC with Fresolimumab, a TGF-β1 neutralizing antibody, significantly reduced the percentage of polyploid TC after TGF-β1 stimulation (Fig. 3K-M and Supplemental Fig. S6, https://figshare.com/s/4eda5e9e97ba3bd2c469). Treatment with verteporfin, a YAP1 inhibitor, was sufficient to reduce TGF-β1-stimulated polyploidization, implying that TGF-β1 promotes polyploidy *via* YAP1 (Fig. 3N-P). Additionally, treatment with verteporfin prevented the up-regulation of pro-fibrotic genes following TGF-β1 stimulation (Fig. 3Q-T). Collectively, these data proved that TC polyploidization is a self-sustained mechanism mediated by TGF-β1 *via* YAP1 activation.

Polyploid TC interact with macrophages and fibroblasts to sustain tubulointerstitial fibrosis. As TGF-β1 is known to stimulate fibroblast and inflammatory infiltrate activation, we leveraged our dataset generated on mouse kidneys at 2 and 30 days after uni-IRI, to explore the interaction between polyploid TC, fibroblasts and pro-inflammatory populations to promote fibrosis. To do so, we included in our scRNA-seq analysis inflammatory cells, fibroblasts and endothelial cells (Supplemental Fig. S7A, B https://figshare.com/s/4eda5e9e97ba3bd2c469) and checked the expression of Tgf-β1 and its receptors. Polyploid cluster 9 and all interstitial cells produced Tgf-β1, Tgf-βr1 and Tgf-βr2, with macrophages and endothelial cells being the major producers, suggesting a crosstalk among these populations (Fig. 4A). Conversely, the diploid PTC did not express Tgf-β1 (Fig. 4A). To quantify cell–cell communication networks, we then performed ligand-receptor analysis with CellphoneDB. At day 2 after AKI, a total of 2230 interactions took place between all the pairwise combinations of the cell types (Fig. 4B). Interestingly, we found that macrophages are the main target of polyploid cluster 9 and *vice versa*, suggesting an active contribution of polyploid TC in the recruitment of macrophages (Fig. 4B). Moreover, whereas fibroblasts interacted with all populations, polyploid cluster 9 appeared to be a fibroblast preferential target (Fig. 4B). Conversely, polyploid cluster 8 appeared to interact weakly with macrophages, endothelial cells and fibroblasts (Supplemental Fig. S7C https://figshare.com/s/4eda5e9e97ba3bd2c469). To understand the extent of the perturbations of such network, we performed the same analysis at day 30. As expected, interactions of fibroblasts greatly increased with all the populations (67%), while macrophage interactions decrease of a 5%, suggesting a progressive shift in the injury response (Fig. 4C). Importantly, polyploid cluster 8 and 9 were exclusive targets of fibroblasts (Fig. 4D, Supplemental Fig. S7D https://figshare.com/s/4eda5e9e97ba3bd2c469). Remarkably, the interactions of polyploid cluster 9 increased of a 61% specifically only with fibroblasts from day 2 to day 30 (Fig. 4E-G and Supplemental Fig. S7E https://figshare.com/s/4eda5e9e97ba3bd2c469), supporting the existence of a crosstalk between

409 fibroblasts and polyploid TC that progressively grows after AKI. Moreover, a detailed analysis of the
410 top changing reactions between the polyploid cluster 9 and fibroblasts confirmed a dominant role of
411 Tgf-β1 signaling (TGFB1-AR) and pro-fibrotic pathways (COL4A1-Integrin a1b1, COL5A2- Integrin
412 a1b1, COL6A3- Integrin a1b1, FN1-Integrin aVb1) (Fig. 4G and Supplemental Fig. S7F
413 https://figshare.com/s/4eda5e9e97ba3bd2c469). The same analysis performed between day 2 and day
414 30 in polyploid cluster 9 confirmed a progressive shift in the injury response, featuring the increase of
415 pro-fibrotic pathways along with the attenuation of pro-inflammatory pathways at day 30 after AKI
416 (Supplemental Fig. S7G https://figshare.com/s/4eda5e9e97ba3bd2c469). Collectively, these findings
417 reveal the existence of a crosstalk between polyploid TC, macrophages and fibroblasts and indicate that
418 polyploid cluster 9 progressively modifies its state, passing from a pro-inflammatory profile at day 2
419 recruiting macrophages to a pro-fibrotic profile at day 30 after AKI, activating fibroblasts. Of note, the
420 observation that polyploid TC are progressively specific targets of fibroblasts, suggests a role for these
421 cells in stimulating the continuous recruitment of polyploid TC overtime and the acquisition of a
422 fibrogenic phenotype, driving CKD. To corroborate the *in vivo* observation, we set up co-cultures
423 between hPTC and human monocytes or fibroblasts *in vitro*. Specifically, we treated hPTC with
424 hydrogen peroxide to mimic the hypoxic injury or TGF- β1 and then we co-coltured them with human
425 monocytes or fibroblasts, respectively. After co-culturing with hPTC, monocytes acquired a pro-
426 inflammatory phenotype, as demonstrated by up-regulation of HIF1α, MAF, IL-6 and TGF-β1 in
427 comparison to monocytes cultured alone (Fig. 5A-E), and fibroblasts expressed higher levels of the
428 senescent marker p21, and the pro-fibrotic CCL2, in comparison to fibroblasts cultured alone (Fig. 5F-
429 H). Similar data were obtained with hPTC and macrophages co-cultures, further proving that hPTC
430 interact with macrophages activating pro-fibrotic pathways (Supplemental Fig. S8,
431 https://figshare.com/s/4eda5e9e97ba3bd2c469). Collectively, these results confirmed the existence of a
432 crosstalk between polyploid TC and interstitial cells.

Discussion

Kidney tubule response to AKI is still a matter of debate and has attracted a growing interest in the recent years. Recognition that the tubule is not able to fully regenerate after AKI and that AKI itself is a risk factor for CKD stimulated the identification of previously unknown mechanisms of response within the tubule. Accordingly, our group recently proved the presence of polyploidy in TC after AKI, and proposed them as a primary driver of CKD progression after AKI (4, 12). However, the mechanism linking polyploid TC to fibrosis development, the final manifestation of CKD progression, remains to be clarified. This work extends our previous studies on TC polyploidization and provides novel mechanistic insights, drawing out two main conclusions. First, expression of cell cycle markers identifies a population of DNA damaged polyploid TC rather than proliferating TC. Indeed, using scRNA-seq we showed that PTC that appeared to be actively cycling based on traditional cell cycle markers were rather polyploid TC with DNA damage. These cells were characterized by both polyploidy regulators and cell cycle inhibitors such as p21, which was found to promote TC polyploidization in a model of karyomegalic interstitial nephritis (6). In this model, TC are unable to successfully repair DNA damage promoting CKD (6). As in the heart and in the liver, the archetypes of polyploid organs, DNA damage in TC likely promotes polyploidization to endure oxidative stress (20, 21). Accordingly, polyploid TC tend to accumulate genome instability and survive after AKI, while diploid TC do not. Therefore, polyploidization may signal the presence of DNA damage, offering an opportunity for novel therapies, also in the kidney.

Secondly, we showed that polyploid TC with DNA damage acquire a progressive pro-fibrotic profile characterized by TGF-β1 expression during the chronic phase after injury. Accordingly, DNA damage triggers TGF-β1 production initiating a vicious circle that leads to fibroblast activation and fibrosis development in the intestine (11). Importantly, we demonstrated that TGF-β1 directly promotes polyploidization *via* YAP1, thus suggesting TC polyploidization is a self-sustained mechanism

promoted by TGF-β1. A similar mechanism was shown in the liver (9). The ligand-receptor analysis further revealed that TGF-β1 signaling fosters a reciprocal activation loop among polyploid TC, macrophages and fibroblasts. It is reasonable to hypothesize that TGF-β1 secreted by polyploid TC and interstitial cells may be acting in an autocrine and paracrine fashion to the surrounding cells. Specifically, as diploid TC are also a target of TGF-β signaling, TGF-β1 can act to continuously increase the fraction of polyploid TC after AKI. This results in the activation of fibroblasts, which in turn interact with polyploid TC to maintain this loop. The existence of a preferential crosstalk among polyploid TC, macrophages and fibroblasts confirms a role for polyploid TC in promoting and accelerating the development of tubulointerstitial fibrosis in CKD. These results contribute to the ongoing revision of the paradigm of kidney tubule response to AKI. Previous studies concluded that after AKI, the mechanism driving CKD was the G2/M cell cycle arrest of TC in response to damage. However, we and others recently argued against this hypothesis (4, 12, 22), disproving a G2/M-arrested state of TC after injury and suggesting that arrested TC rather represent polyploid TC (4, 6, 12). Collectively, previous studies in conjunction with the results reported in this, suggest that G2/M-arrested cells and polyploid TC are the same rather than distinct TC states. Therefore, polyploid TC represent the apical determinant for the long-term outcome to kidney insults further reinforcing the central role played by kidney tubule in CKD and can represent a valid therapeutic target to slow its progression.

Supplemental Material available at

URL number: https://figshare.com/s/4eda5e9e97ba3bd2c469

DOI number: https://doi.org/10.6084/m9.figshare.22200187

References

1. **Kellum JA, Romagnani P, Ashuntantang G, Ronco C, Zarbock A, and Anders HJ**. Acute kidney injury. *Nat Rev Dis Primers* 7: 52, 2021.

2. **Humphreys BD**. Mechanisms of Renal Fibrosis. *Annu Rev Physiol* 80: 309-326, 2018.

3. **Allinovi M, De Chiara L, Angelotti ML, Becherucci F, and Romagnani P**. Anti-fibrotic treatments: A review of clinical evidence. *Matrix Biol* 68-69: 333-354, 2018.

4. **De Chiara L, Conte C, Semeraro R, Diaz-Bulnes P, Angelotti ML, Mazzinghi B, Molli A, Antonelli G, Landini S, Melica ME, Peired AJ, Maggi L, Donati M, La Regina G, Allinovi M, Ravaglia F, Guasti D, Bani D, Cirillo L, Becherucci F, Guzzi F, Magi A, Annunziato F, Lasagni L, Anders HJ, Lazzeri E, and Romagnani P**. Tubular cell polyploidy protects from lethal acute kidney injury but promotes consequent chronic kidney disease. *Nat Commun* 13: 5805, 2022.

5. **Taguchi K, Elias BC, Sugahara S, Sant S, Freedman BS, Waikar SS, Pozzi A, Zent R, Harris RC, Parikh SM, and Brooks CR**. Cyclin G1 induces maladaptive proximal tubule cell dedifferentiation and renal fibrosis through CDK5 activation. *J Clin Invest* 132: 2022.

6. **Airik M, Phua YL, Huynh AB, McCourt BT, Rush BM, Tan RJ, Vockley J, Murray SL, Dorman A, Conlon PJ, and Airik R**. Persistent DNA damage underlies tubular cell polyploidization and progression to chronic kidney disease in kidneys deficient in the DNA repair protein FAN1. *Kidney Int* 102: 1042-1056, 2022.

7. **Meng XM, Nikolic-Paterson DJ, and Lan HY**. TGF-beta: the master regulator of fibrosis. *Nat Rev Nephrol* 12: 325-338, 2016.

8. **Muto Y, Dixon EE, Yoshimura Y, Wu H, Omachi K, Ledru N, Wilson PC, King AJ, Eric Olson N, Gunawan MG, Kuo JJ, Cox JH, Miner JH, Seliger SL, Woodward OM, Welling PA, Watnick TJ, and Humphreys BD**. Defining cellular complexity in human autosomal dominant polycystic kidney disease by multimodal single cell analysis. *Nat Commun* 13: 6497, 2022.

9. **De Santis Puzzonia M, Cozzolino AM, Grassi G, Bisceglia F, Strippoli R, Guarguaglini G, Citarella F, Sacchetti B, Tripodi M, Marchetti A, and Amicone L**. TGFbeta Induces Binucleation/Polyploidization in Hepatocytes through a Src-Dependent Cytokinesis Failure. *PLoS One* 11: e0167158, 2016.

10. **Wen QJ, Yang Q, Goldenson B, Malinge S, Lasho T, Schneider RK, Breyfogle LJ, Schultz R, Gilles L, Koppikar P, Abdel-Wahab O, Pardanani A, Stein B, Gurbuxani S, Mullally A, Levine RL, Tefferi A, and Crispino JD**. Targeting megakaryocytic-induced fibrosis in myeloproliferative neoplasms by AURKA inhibition. *Nat Med* 21: 1473-1480, 2015.

11. **Li Y, Liu Y, Chiang YJ, Huang F, Li Y, Li X, Ning Y, Zhang W, Deng H, and Chen YG**. DNA Damage Activates TGF-beta Signaling via ATM-c-Cbl-Mediated Stabilization of the Type II Receptor TbetaRII. *Cell Rep* 28: 735-745 e734, 2019.

12. **Lazzeri E, Angelotti ML, Peired A, Conte C, Marschner JA, Maggi L, Mazzinghi B, Lombardi D, Melica ME, Nardi S, Ronconi E, Sisti A, Antonelli G, Becherucci F, De Chiara L, Guevara RR, Burger A, Schaefer B, Annunziato F, Anders HJ, Lasagni L, and Romagnani P**. Endocycle-related tubular cell hypertrophy and progenitor proliferation recover renal function after acute kidney injury. *Nat Commun* 9: 1344, 2018.

13. **Mort RL, Ford MJ, Sakaue-Sawano A, Lindstrom NO, Casadio A, Douglas AT, Keighren MA, Hohenstein P, Miyawaki A, and Jackson IJ**. Fucci2a: a bicistronic cell cycle reporter that allows Cre mediated tissue specific expression in mice. *Cell Cycle* 13: 2681-2696, 2014.

14. **Peired AJ, Antonelli G, Angelotti ML, Allinovi M, Guzzi F, Sisti A, Semeraro R, Conte C, Mazzinghi B, Nardi S, Melica ME, De Chiara L, Lazzeri E, Lasagni L, Lottini T, Landini S, Giglio S, Mari A, Di Maida F, Antonelli A, Porpiglia F, Schiavina R, Ficarra V, Facchiano D, Gacci M, Serni S, Carini M, Netto GJ, Roperto RM, Magi A, Christiansen CF, Rotondi M, Liapis H, Anders HJ, Minervini A, Raspollini MR, and Romagnani P**. Acute kidney injury promotes

development of papillary renal cell adenoma and carcinoma from renal progenitor cells. *Sci Transl Med* 12: 2020.

15. **Greco R, Qu H, Qu H, Theilhaber J, Shapiro G, Gregory R, Winter C, Malkova N, Sun F, Jaworski J, Best A, Pao L, Hebert A, Levit M, Protopopov A, Pollard J, Bahjat K, Wiederschain D, and Sharma S**. Pan-TGFbeta inhibition by SAR439459 relieves immunosuppression and improves antitumor efficacy of PD-1 blockade. *Oncoimmunology* 9: 1811605, 2020.

16. **Tirosh I, Izar B, Prakadan SM, Wadsworth MH, 2nd, Treacy D, Trombetta JJ, Rotem A, Rodman C, Lian C, Murphy G, Fallahi-Sichani M, Dutton-Regester K, Lin JR, Cohen O, Shah P, Lu D, Genshaft AS, Hughes TK, Ziegler CG, Kazer SW, Gaillard A, Kolb KE, Villani AC, Johannessen CM, Andreev AY, Van Allen EM, Bertagnolli M, Sorger PK, Sullivan RJ, Flaherty KT, Frederick DT, Jane-Valbuena J, Yoon CH, Rozenblatt-Rosen O, Shalek AK, Regev A, and Garraway LA**. Dissecting the multicellular ecosystem of metastatic melanoma by single-cell RNA-seq. *Science* 352: 189-196, 2016.

17. **Fang Z, Liu X, and Peltz G**. GSEApy: a comprehensive package for performing gene set enrichment analysis in Python. *Bioinformatics* 2022.

18. **Hagberg A, Pieter Swart, and Daniel S Chult**. Exploring network structure, dynamics, and function using NetworkX. 2008.

19. **Prakash V, Carson BB, Feenstra JM, Dass RA, Sekyrova P, Hoshino A, Petersen J, Guo Y, Parks MM, Kurylo CM, Batchelder JE, Haller K, Hashimoto A, Rundqivst H, Condeelis JS, Allis CD, Drygin D, Nieto MA, Andang M, Percipalle P, Bergh J, Adameyko I, Farrants AO, Hartman J, Lyden D, Pietras K, Blanchard SC, and Vincent CT**. Ribosome biogenesis during cell cycle arrest fuels EMT in development and disease. *Nat Commun* 10: 2110, 2019.

20. **Gentric G, Maillet V, Paradis V, Couton D, L'Hermitte A, Panasyuk G, Fromenty B, Celton-Morizur S, and Desdouets C**. Oxidative stress promotes pathologic polyploidization in nonalcoholic fatty liver disease. *J Clin Invest* 125: 981-992, 2015.

21. **Derks W, and Bergmann O**. Polyploidy in Cardiomyocytes: Roadblock to Heart Regeneration? *Circ Res* 126: 552-565, 2020.

22. **Gerhardt LMS, Liu J, Koppitch K, Cippa PE, and McMahon AP**. Single-nuclear transcriptomics reveals diversity of proximal tubule cell states in a dynamic response to acute kidney injury. *Proc Natl Acad Sci U S A* 118: 2021.

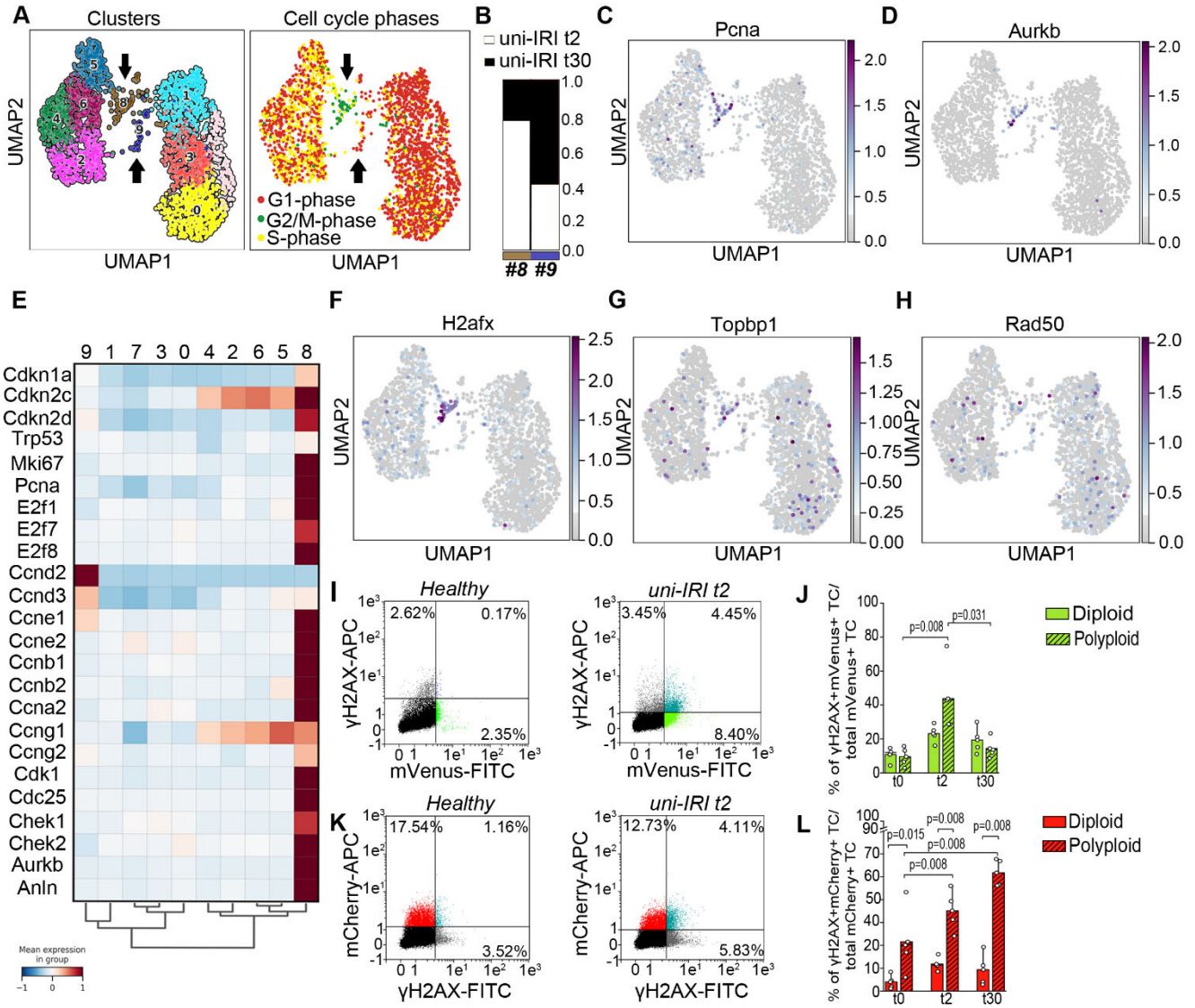

Figure 1. Polyploid TC with DNA damage accumulate after injury *in vivo*. (A) UMAP of cluster distribution and of cell cycle distribution of mouse PTC at day 2 and 30 after uni-IRI. (B) Barplot showing experimental time distribution in cluster 8 and cluster 9. (C) UMAP distribution of cell cycle activation (Pcna), and (D) cell cycle progression (Aurkb) genes. (E) Matrixplot showing expression of genes involved in cell cycle progression and inhibition. (F-H) UMAP distribution of DNA damage markers H2afx, Topbp1 and Rad50. (I) Representative FACS analysis and gating strategy of mVenus+ TC stained for γH2AX in healthy and 2 days after uni-IRI (n=5). (J) Percentage of γH2AX+/mVenus+ TC diploid (i.e., actively proliferating) and polyploid (i.e., undergoing endoreplication). (K)

569 Representative FACS analysis and gating strategy of mCherry+ TC stained for γH2AX in healthy and 2
570 days after uni-IRI (n=5). (L) Percentage of γH2AX+/mCherry+ TC diploid and polyploid showing
571 accumulation over time in the polyploid population. Statistical significance was calculated by two-
572 sided Mann-Whitney test; numbers on graphs represent exact p values. Bar plots: line = mean,
573 whisker = outlier (coef. 1.5). TC: tubular cells; uni-IRI: unilateral-ischemia reperfusion injury.
574

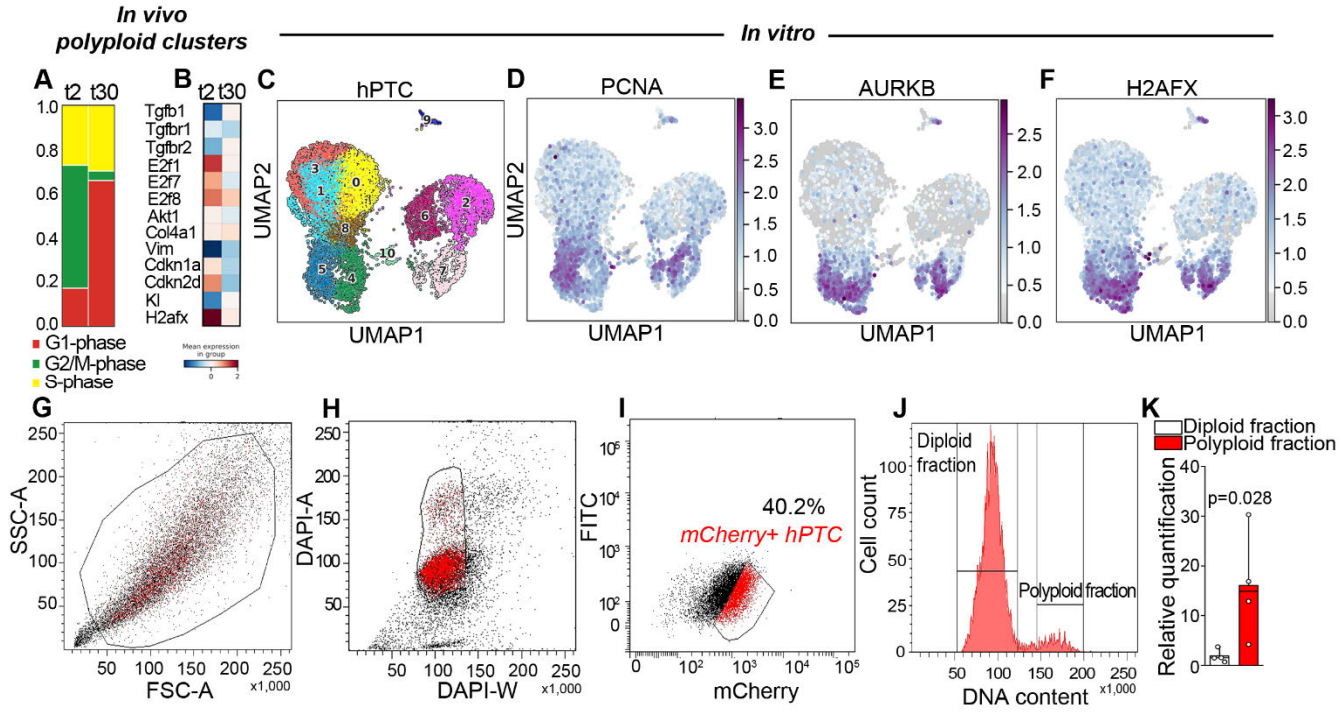

Figure 2. Polyploid TC with DNA damage are pro-fibrotic and actively produce TGF-β1 *in vitro*. (A) Barplot showing cell cycle phases in mouse polyploid clusters (8 and 9) divided in day 2 (t2) and 30 (t30) after uni-IRI. (B) Matrixplot of mouse polyploid clusters (8 and 9) divided in day 2 (t2) and 30 (t30) after uni-IRI, showing TGF-β1 and its receptors. (C) UMAP showing human proximal tubular epithelial cell (hPTC) clusters. (D) UMAP distribution of cell cycle activation (PCNA), and (E) cell cycle progression (AURKB) genes. (F) UMAP distribution of DNA damage marker H2AFX. (G-I) FACS analysis of mCherry-hPTC (cells in the G1 phase) showing the gating strategy for sorting. (J) Cell cycle distribution of diploid and polyploid mCherry-hPTC. A representative experiment out of 4 is shown. (K) TGF-β1 gene expression in sorted polyploid mCherry-hPTC over diploid mCherry-hPTC (n=4). Statistical significance was calculated by two-sided Mann-Whitney test; numbers on graph represent exact *p* value. Bar plots: line = mean, whisker = outlier (coef. 1.5).

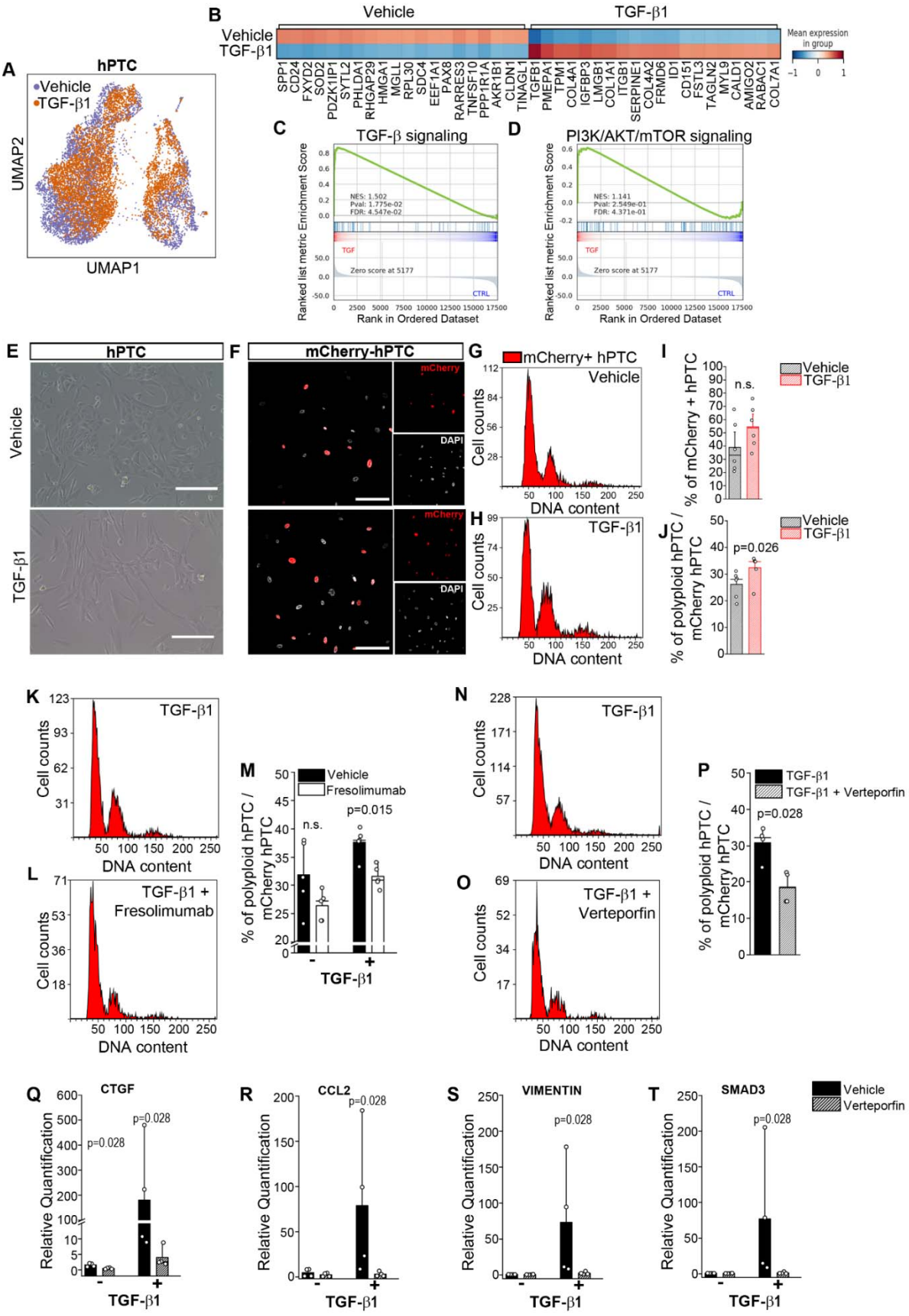

588

Figure 3. Polyploidization is a self-sustained mechanism stimulated by TGF-β1. (A) UMAP showing sample distribution. (B) First twenty characteristic genes of vehicle treated hPTC and TGF-β1 treated hPTC. (C) Gene set enrichment analysis showing activation of TGF-β pathway. (D) Gene set enrichment analysis showing activation of AKT pathway, one of the regulator of polyploidy in PTC. (E) Representative brightfield picture of mCherry-hPTC treated with vehicle (upper panel) or TGF-β1 (lower panel) for 48h. Bar 400µm (F) Representative picture of mCherry-hPTC treated with vehicle (upper panel) or TGF-β1 (lower panel) for 48h. DAPI counterstains nuclei. Bar 150µm. (G) Cell cycle distribution of vehicle treated mCherry-hPTC. (H) Cell cycle distribution of TGF-β1 treated mCherry-hPTC. (I) Total percentage of mCherry-hPTC in vehicle and TGF-β1 conditions (n=6). (J) Percentage of polyploid mCherry-hPTC in vehicle-treated or TGF-β1-treated culture (n=6). (K) Cell cycle distribution of TGF-β1 treated mCherry-hPTC. (L) Cell cycle distribution of TGF-β1 and Fresolimumab treated mCherry-hPTC. (M) Total percentage of mCherry-hPTC in vehicle and TGF-β1 conditions (n=5). (N) Cell cycle distribution of TGF-β1 treated mCherry-hPTC. (O) Cell cycle distribution of TGF-β1 and Verteporfin treated mCherry-hPTC. (P) Total percentage of mCherry-hPTC in TGF-β1 and TGF-β1 with Verteporfin conditions (n=4). (Q-T) RealTime PCR analysis of CTGF, CCL2, VIMENTIN and SMAD3, following TGF-β1 stimulation and verteporfin treatment (n=4). Statistical significance was calculated by two-sided Mann-Whitney test; numbers on graphs represent exact *p* values. Bar plots: line = mean, whisker = outlier (coef. 1.5). hPTC: human proximal tubular epithelial cells.

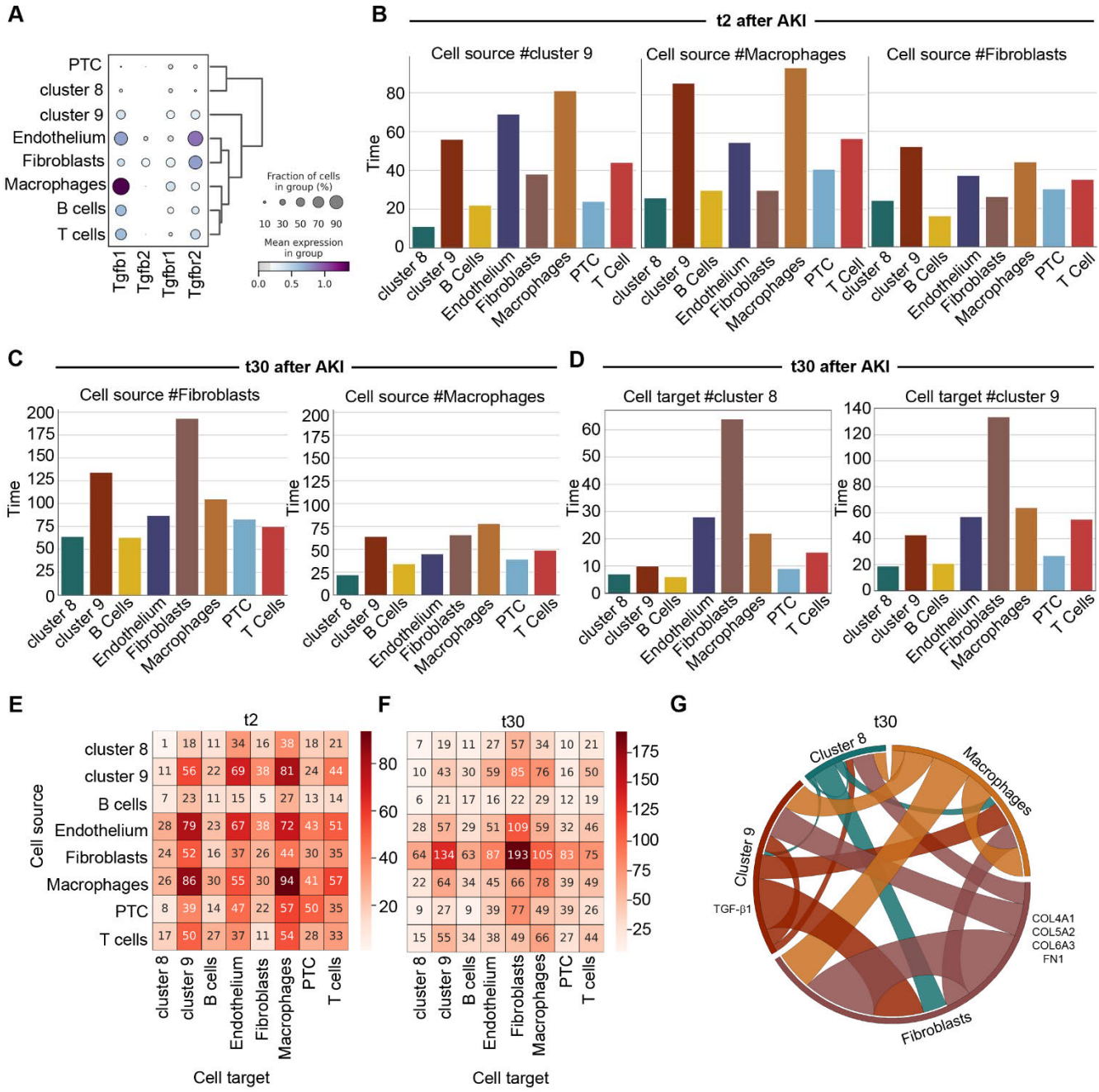

609

610 **Figure 4. Polyploid TC interact with macrophages and fibroblasts to sustain tubulointerstitial**
611 **fibrosis.** (A) Dotplot showing Tgf-β1, Tgf-β2, Tgf-βr1 and Tgf-βr2 distribution in all the mouse
612 populations retrieved from kidneys 2 and 30 days after uni-IRI. (B) Barplots reporting the number of
613 interactions occurring 2 days after uni-IRI between cluster 9, macrophages and fibroblasts as source
614 and all the cell types. (C) Barplots reporting the number of interactions occurring 30 days after uni-IRI

between fibroblasts and macrophages as source and all the cell types. (D) Barplots reporting the number of interactions occurring 30 days after uni-IRI between the cluster 8 and 9 cells as target, and all the cell types. (E, F) Heatmap reporting the number of interactions between cell types, as source and target, at day 2 and 30 after uni-IRI. (G) Circos plot of ligand-receptor interactions among polyploid cluster 9, 8, macrophages and fibroblasts in kidneys at day 30 after uni-IRI. The populations producing the putative ligand (TGFB1-AR, COL4A1-Integrin a1b1, COL5A2-Integrin a1b1, COL6A3-Integrin a1b1, FN1-Integrin aVb1) are shown. PTC: proximal tubular cells.

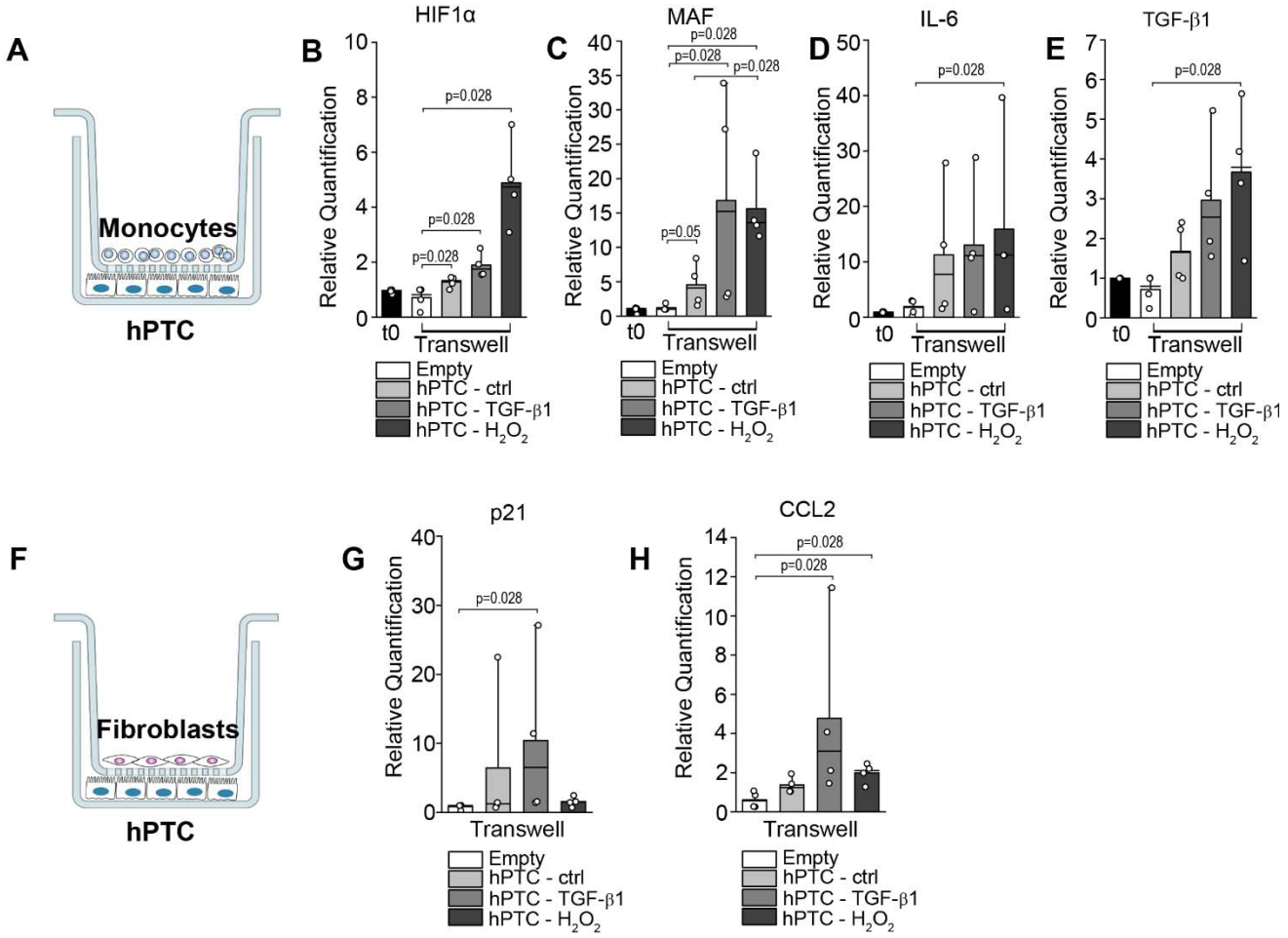

623

624 **Figure 5. TC interact with monocytes and fibroblasts activating pro-inflammatory and pro-**
625 **fibrotic pathways.** (A) Schematic representation of experimental plan for co-culture with monocytes.
626 (B) RealTime PCR analysis of HIF1α, (C) MAF, (D) IL-6 and (E) TGF-β1 in monocytes following co-
627 culture with non-stimulated hPTC and after TGF-β1 and H_2O_2 treatment (n=4). (F) Schematic
628 representation of experimental plan for co-culture with fibroblasts. (G, H) RealTime PCR analysis of
629 p21 and CCL2 in fibroblasts following co-culture with non-stimulated hPTC and after TGF-β1 and
630 H_2O_2 treatment (n=4). Statistical significance was calculated by two-sided Mann-Whitney test;
631 numbers on graphs represent exact *p* values. Bar plots: line = mean, whisker = outlier (coef. 1.5). t0:

632 monocytes after purification, hPTC: human proximal tubular epithelial cells, empty: transwell with
633 monocytes or fibroblasts without hPTC.
634
635
636

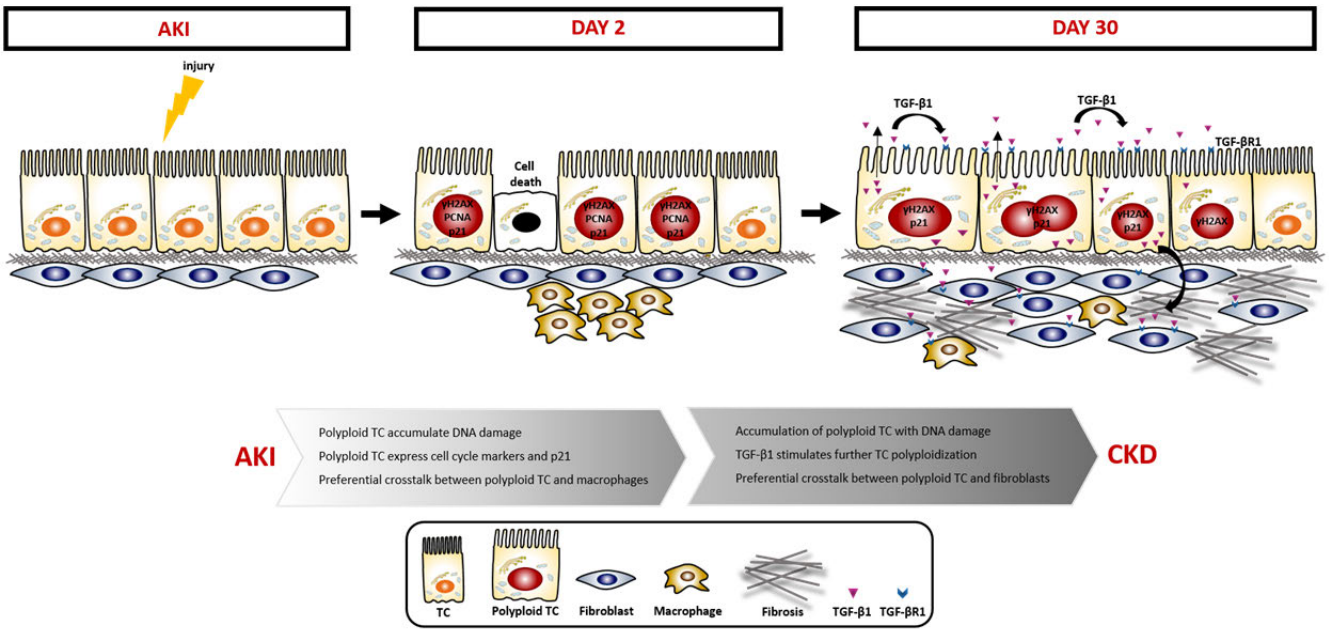

637

638 **Figure 6. Schematic representation of polyploid TC response to AKI.** In response to AKI TC
639 undergo polyploidization. Polyploid cells are characterized by DNA damage, cell cycle markers and
640 p21 expression 2 days after AKI. In the long term, polyploid TC start to secrete TGF-β1, which triggers
641 a feedback loop to generate further polyploid TC and activate macrophages and fibroblasts. AKI: Acute
642 Kidney Injury, CKD: Chronic Kidney Disease, TGF-β1: Transforming Growth Factor 1, TC: Tubular
643 Cells, γH2AX: H2A Histone family member X, p21: CDKN1A, TGF-βR1: Transforming Growth
644 Factor β Receptor1.

645

Acknowledgements.

This research was funded by the European Union's Marie Sklodowska-Curie fellowship program to L.D.C. This study was also funded by PRIN: progetti di ricerca di interesse nazionale (2017T95E9X) to P.R. L.D.C. is also the recipient of a L'Oreal-Unesco for women in science award.

Conflict of Interest Statement.

The Authors declare no conflict of interest.

Authors' Contributions

L.D.C., E.L., and P.R. designed the study and interpreted the data. L.D.C. performed or supervised all the experiments. R.S. analyzed all the data from the scRNA-seq analysis. B.M. carried out all scRNA-seq and assisted with data analysis. S.L. validated and sequenced the single-cell libraries. A. M. performed *in vivo* experiments and prepared samples for flow cytometry. M.L.A and G.A. designed and performed immunofluorescence and confocal microscopy. M.E.M performed in vitro experiments. L.M. performed cell sorting experiments. C.C. performed flow cytometry. A.J.P. carried out mouse experiments. L.C. assisted with statistical analysis and critically revised the manuscript. V.R. helped with the in vitro experiments. A.M. helped with scRNA-seq analysis. F.A. assisted and advised on flow cytometry data interpretation. P.R. critically revised and edited the manuscript and advised on data interpretation. E.L. and L.D.C. wrote the manuscript and organized the figures. All authors read and approved the final manuscript.

Funding

This research was funded by the European Union's Marie Sklodowska-Curie fellowship program to L.D.C., grant agreement No. 845774. This study was also funded by PRIN: progetti di ricerca di interesse nazionale (2017T95E9X) to P.R.

Data Availability Statement

Data used is available from the corresponding author upon reasonable request. Processed data for the human scRNA-seq libraries generated in this study have been deposited in the Gene Expression Omnibus (GEO) database under accession code (will be provided upon acceptance).

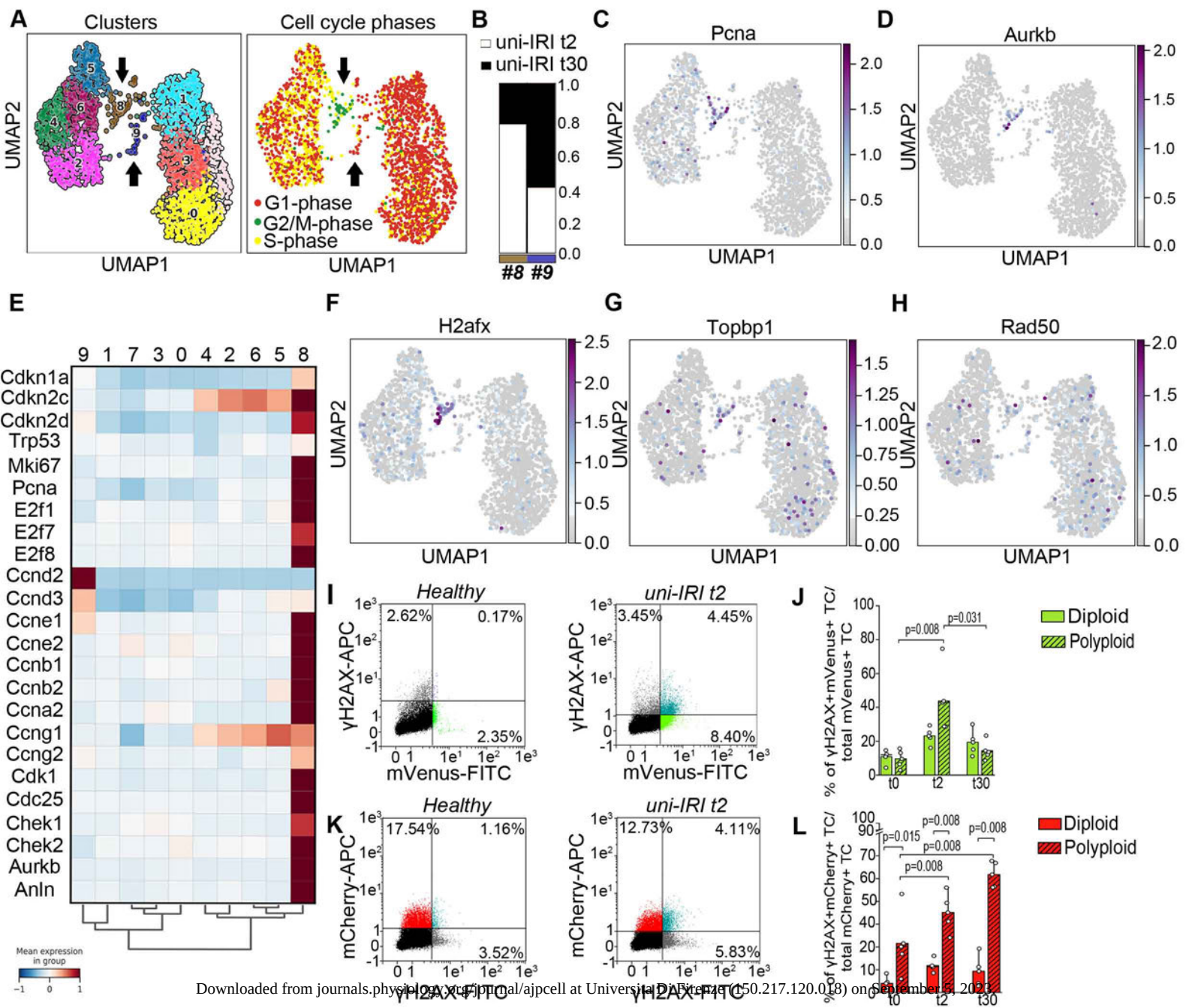

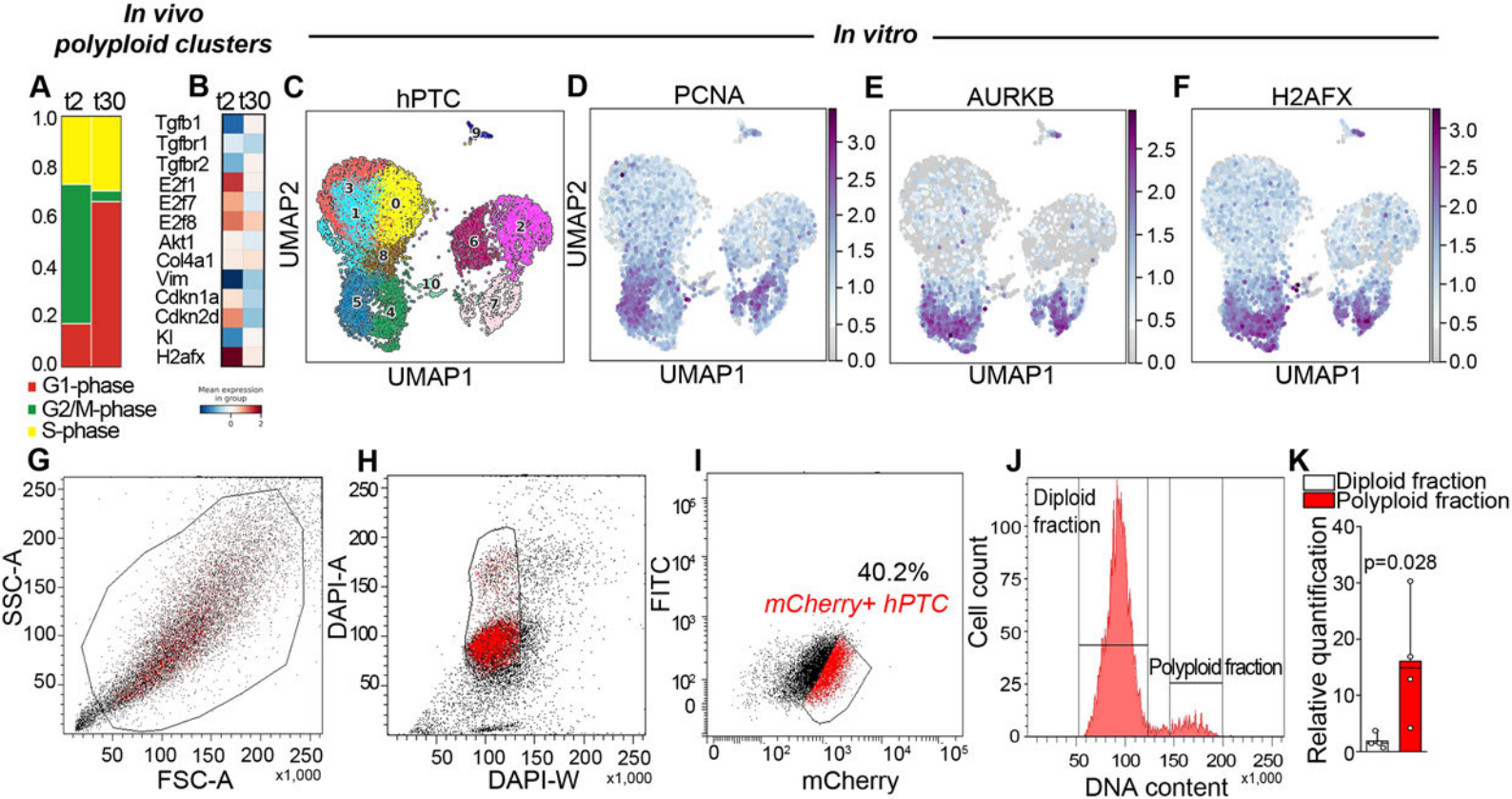

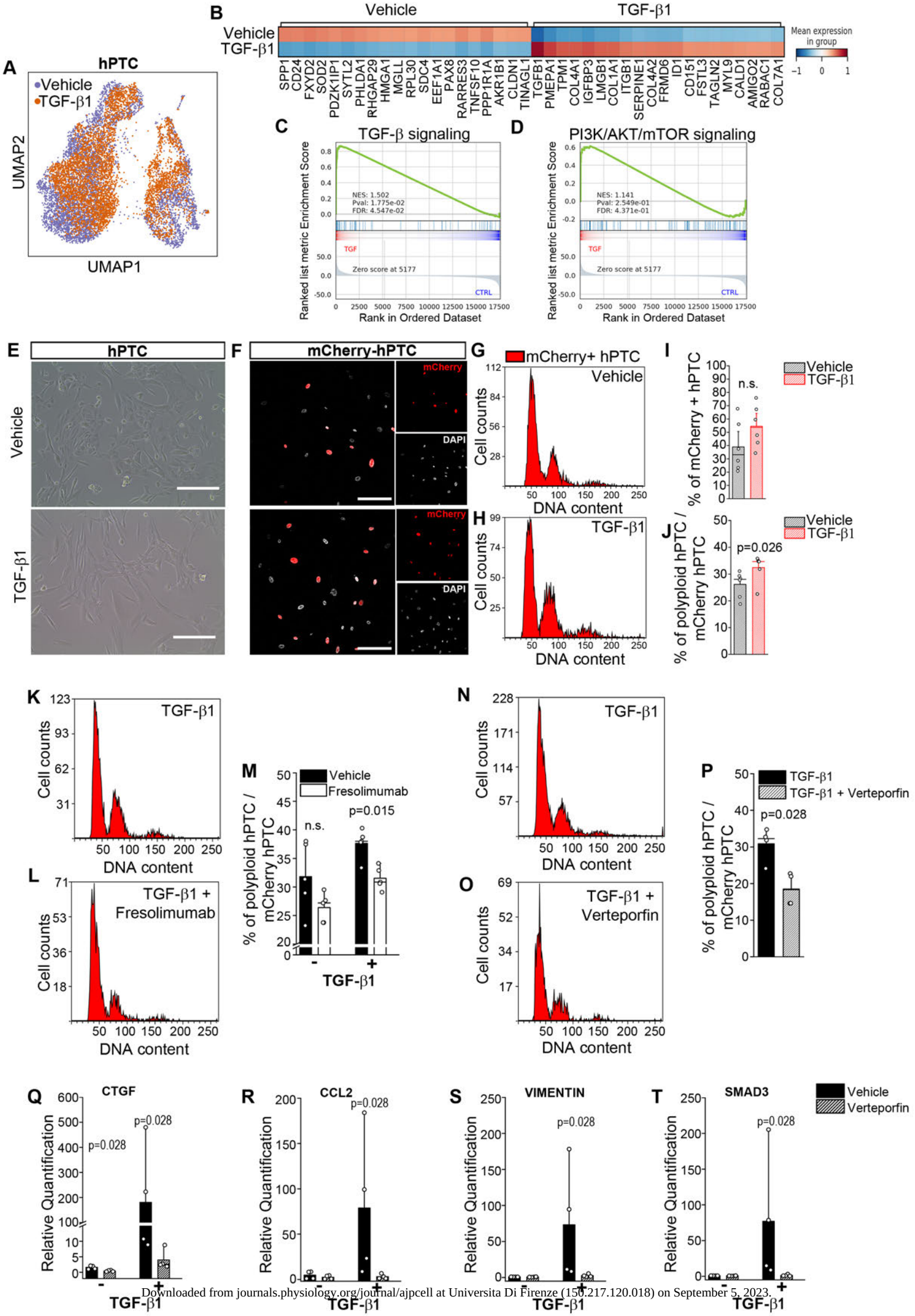

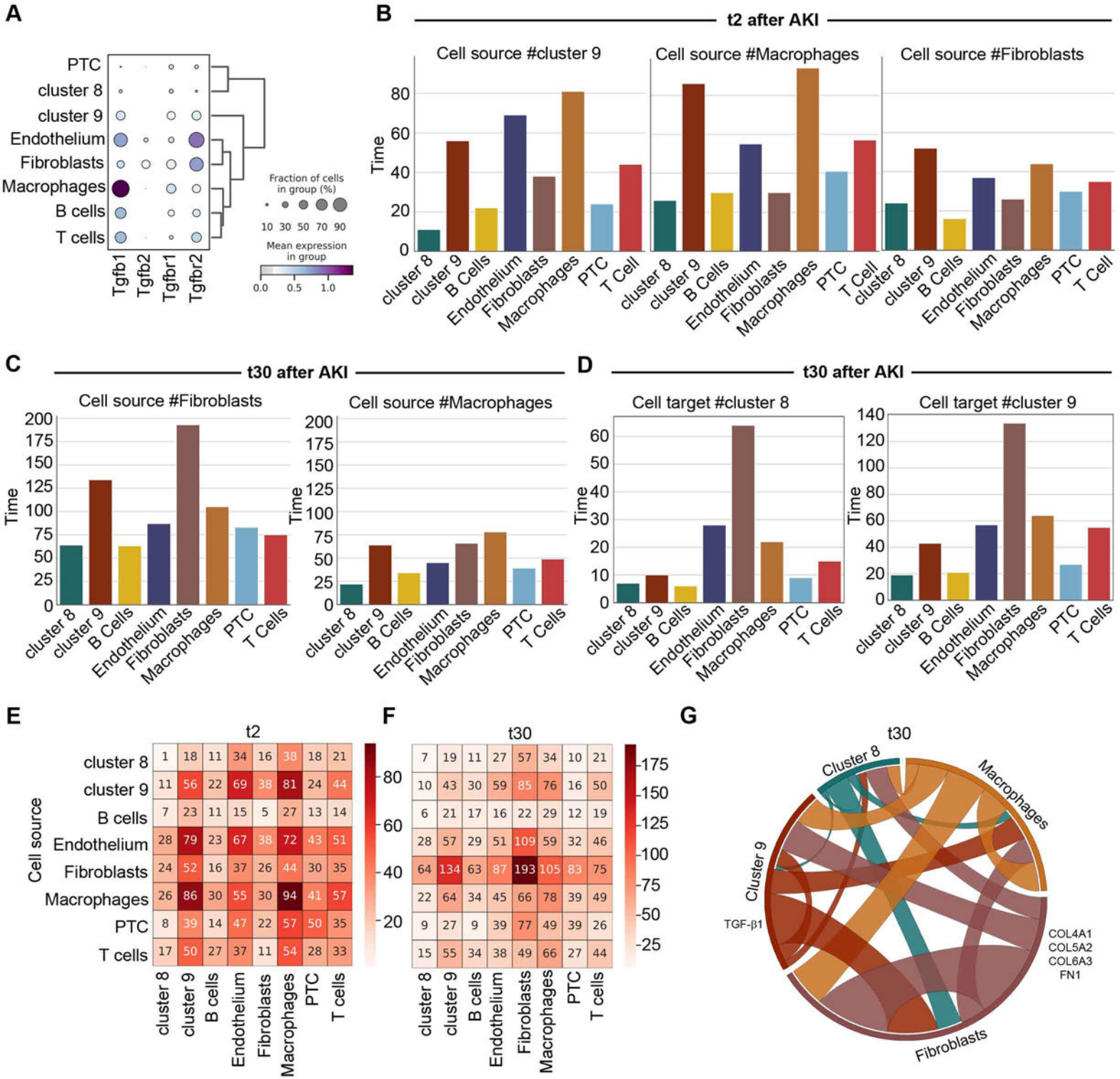

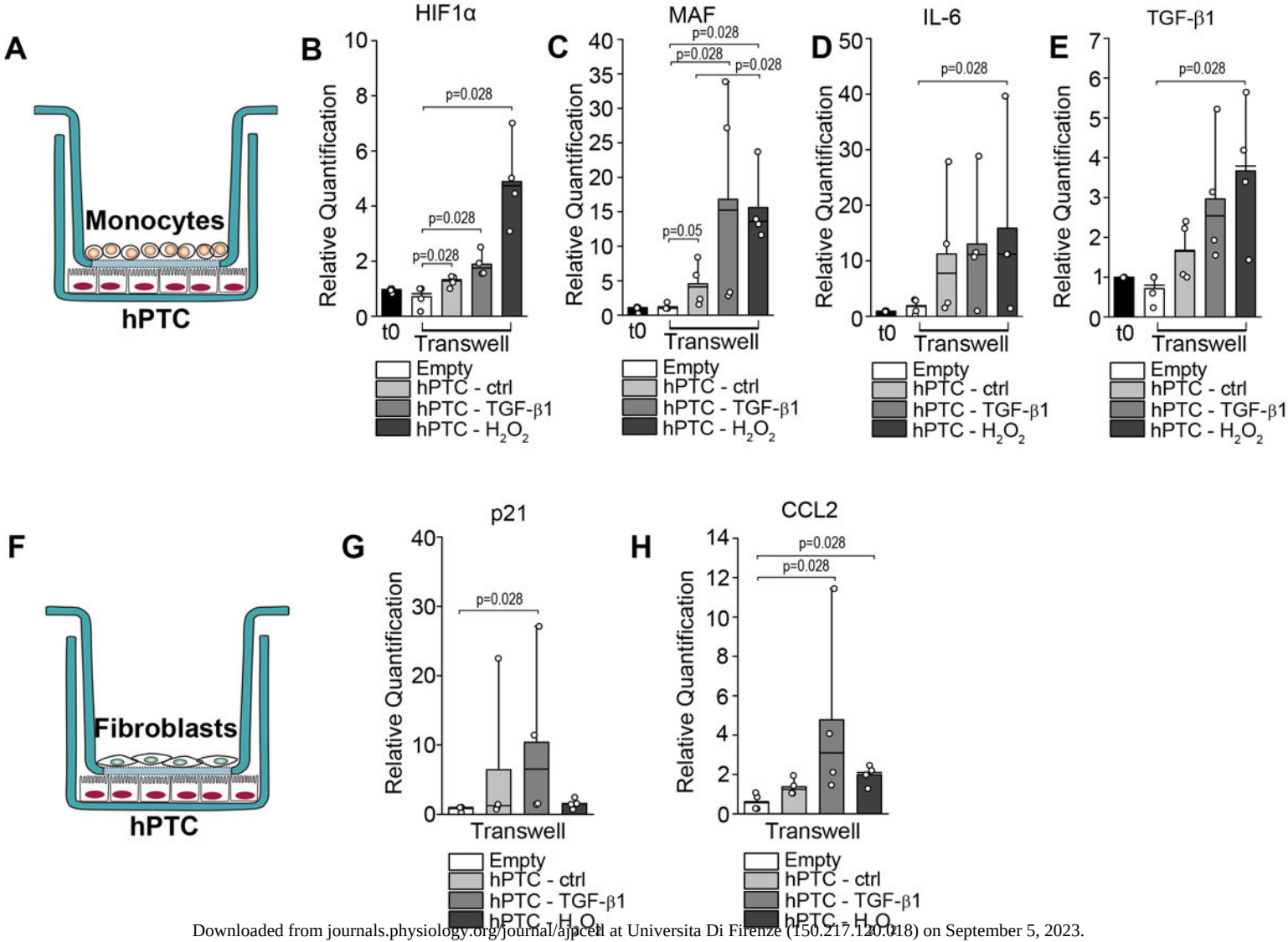

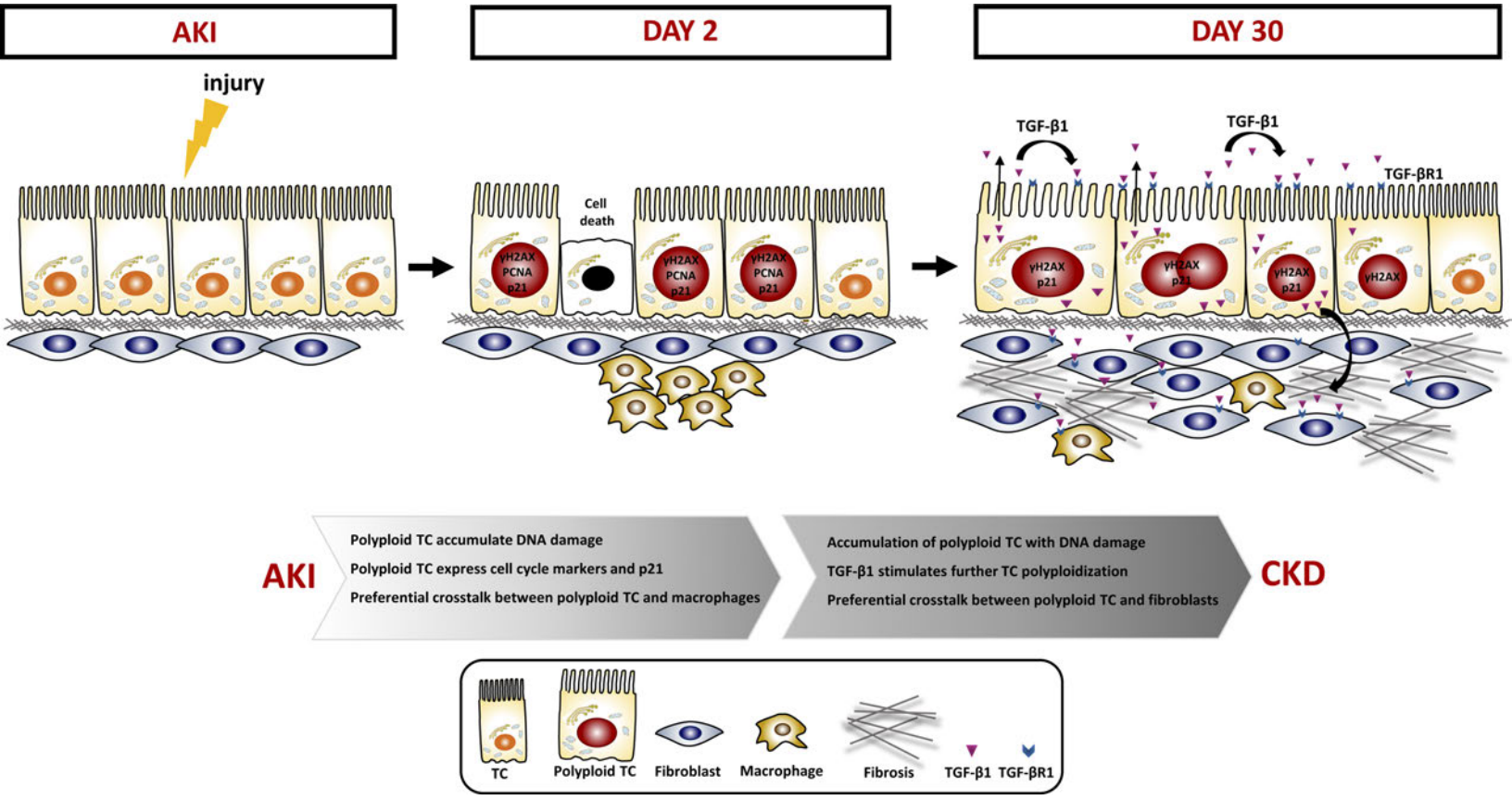

Polyploid tubular cells promote fibrosis *via* TGF-β1

RESULTS

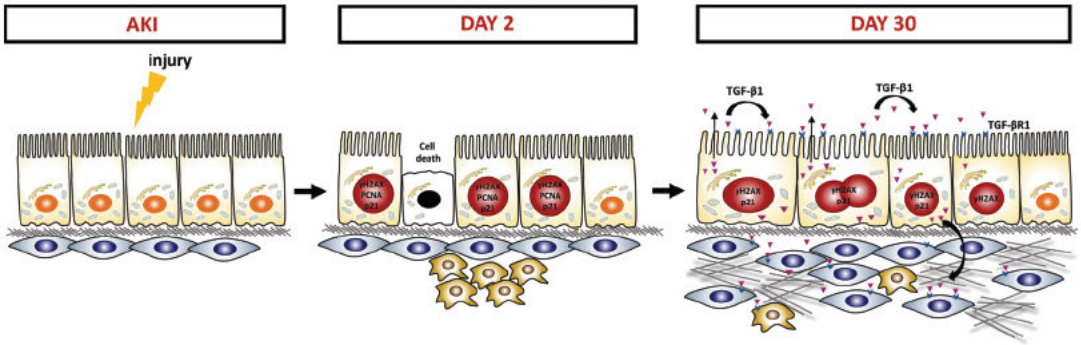

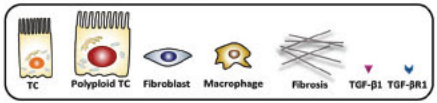

CONCLUSION

Polyploid TC with DNA damage acquire a progressive pro-fibrotic profile characterized by TGF-β1 expression, which generates further polyploid TC. Moreover, TGF-β1 triggers a crosstalk among polyploid TC, macrophages and fibroblasts, driving fibrosis.

AMERICAN JOURNAL OF PHYSIOLOGY
CELL PHYSIOLOGY © 2023

american physiological society